HHS Public Access

Author manuscript

Seizure. Author manuscript; available in PMC 2019 November 01.

Published in final edited form as:

Seizure. 2018 November ; 62: 3–10. doi:10.1016/j.seizure.2018.09.005.

Subfield-specific Tractography of the Hippocampus in Epilepsy Patients at 7 Tesla

John W. Rutland[1,2], **Rebecca E. Feldman, PhD**[1,2], **Bradley N. Delman, MD**[2], **Fedor Panov, MD**[3], **Madeline C. Fields, MD**[4], **Lara V. Marcuse, MD**[4], **Patrick R. Hof, MD**[5], **Hung-Mo Lin, ScD**[6], and **Priti Balchandani, PhD**[1,2]

[1]Translational and Molecular Imaging Institute, Icahn School of Medicine at Mount Sinai, New York, New York, United States

[2]Department of Radiology, Icahn School of Medicine at Mount Sinai, New York, New York, United States

[3]Department of Neurosurgery, Mount Sinai Hospital, New York, New York, United States

[4]Department of Neurology, Mount Sinai Hospital, New York, New York, United States

[5]Department of Neuroscience, Mount Sinai Hospital, New York, New York, United States

[6]Department of Population Health Science and Policy, Mount Sinai Hospital, New York, New York, United States

Abstract

Purpose—MRI-negative epilepsy patients could benefit from advanced imaging techniques such as high-resolution diffusion magnetic resonance imaging (dMRI). Our aim was to perform hippocampal subfield-specific tractography and quantify connectivity of the subfields in MRI-negative patients. Abnormal connectivity of the hippocampal subfields may help inform seizure focus hypothesis and provide information to guide surgical intervention.

Methods—Hippocampal structural imaging and dMRI was acquired in 25 drug resistant MRI-negative patients and 25 healthy volunteers. The hippocampi of each subject was segmented on high-resolution structural images and dMRI-based probabilistic tractography was performed in each subfield. The degrees of connectivity and fiber densities of the hippocampal subfields were quantified and compared between epilepsy patients and healthy volunteers.

Results—We were able to perform subfield-specific hippocampal tractography in each subject that participated in this study. These methods identified some hippocampal subfields that are abnormally connected in MRI-negative patients. In particular patients suspected of left temporal

Corresponding Author: John Rutland, Translational and Molecular Imaging Institute, Icahn School of Medicine at Mount Sinai, 1470 Madison Avenue; Floor 1, New York, NY 10129, jack.rutland@mssm.edu, Tel: 212-824-8471, Fax: 646-537-9589.

Disclosures of conflicts of interest

The remaining authors do not have any conflicts of interest to disclose.

seizure focus exhibited increased connectivity of certain ipsilateral subfields, especially the subiculum, presubiculum, and parasubiculum, and reduced connectivity of some contralateral subfields, such as CA1 and subiculum.

Conclusions—Our data suggest that the hippocampal subfields are connected in distinct ways in different types of epilepsy. These results may provide important information that could help inform seizure focus hypothesis and in the surgical treatment of MRI-negative patients. These observations suggest that high-resolution dMRI-based tractography of the hippocampal subfields can detect subtle abnormalities in otherwise normal-appearing MRI-negative patients.

Keywords

Drug resistant epilepsy; diffusion MRI; connectivity; MRI-negative; hippocampus; tractography

1. Introduction

Epilepsy is a common neurological disease, affecting roughly 1% of the population.[1] Approximately 30% to 35% of all epilepsy patients have drug resistant epilepsy (DRE) and their seizures cannot be controlled with medications.[2–5] Neurosurgical intervention is a well-established treatment for patients with DRE.[6] Successful resection of a seizure focus depends electrophysiologic and clinical data as well as lesion identification on pre-surgical magnetic resonance imaging (MRI). However, approximately 25% of epilepsy patients remain “MRI-negative”, with no identifiable lesion or abnormality on clinical scans at 1.5 or 3 T field strengths.[7–10] MRI-negative patients are less likely to achieve seizure freedom after surgical intervention than are MRI-positive patients, and generally have worse prognoses.[11,12]

Localizing the seizure onset zone in MRI-negative patients is especially difficult, and may require intracranial monitoring using subdural grids or stereoelectroencephalography (SEEG) depth electrodes to provide spatial information about seizure foci and propagation pathways.[7,13] Placements of electrodes are determined using non-invasive tools such as MRI, angiography, and scalp EEG.[7,13] Interestingly, MRI-negative epilepsy can be effectively treated with resective surgery or laser ablation if intracranial monitoring successfully localizes the seizure focus.[7,13] The absence of a visible lesion on clinical imaging scans does not necessarily mean the absence of a focal epilepsy network, and further investigation of the epileptic network could improve surgical planning and ultimately outcome for MRI-negative patients.

Since focal epilepsy has received increasing recognition as a network disease, identifying nodes within the network that contribute to seizure activity is an important area of investigation.[15,16] The hippocampus, an archicortical structure in the medial temporal lobe that is composed of cytoarchitecturally distinct subfields, is recognized as a node often involved within epileptic networks. Although small-world network models of epilepsy have demonstrated that individual subfields within the hippocampus participate in seizure activity in different ways[16], the hippocampus has traditionally been treated as a single structure in imaging and clinical settings.[17] The introduction of ultra-high field MRI scanners, coupled with recent software and imaging development has enabled automated segmentation of the

hippocampus *in vivo*.[18–20] Previous studies employing segmentation have found subfield-specific volumetric differences in epilepsy patients compared with healthy volunteers, suggesting that certain subfields may be more susceptible to changes caused by the disease than others and/or that lesions in certain subfields may contribute differently to the seizure mechanism.[19,20] In addition to gross volumetric analysis, understanding of connectivity patterns of differing hippocampal subfields may reveal important details regarding epileptogenic abnormality of the subfields. However, such an analysis has not been performed to elucidate changes that may exist in epilepsy patients.

Diffusion magnetic resonance imaging (dMRI) is a powerful MRI modality that enables the noninvasive *in vivo* mapping of white matter microstructure.[21,22] Myelination of neuronal axons restricts the direction of diffusion, such that water molecules diffuse along the long axis of the fibers more rapidly than they do on the transverse axes.[22] This so-called anisotropic water movement can be used to model the fiber orientation distribution within the white matter tracts, derive measures of fiber integrity, and quantify connectivity between brain regions.[22] Ultra-high field scanners, such as those operating at 7T, provide increased signal to noise ratio (SNR), benefitting dMRI resolution[23], and enabling quantification of hippocampal subfield connectivity.

Since the hippocampus is often the target of epilepsy surgery, characterization of hippocampal subfield connectivity may have significant implications for neurosurgical treatment, especially in temporal lobe epilepsy patients. The extent of temporal resection varies between surgeons, and depends upon variable factors including results of scalp EEG, intracranial EEG, and the preoperative amobarbital (Wada) test.[2] While a more extensive temporal resection maximizes the chances of seizure freedom, it also carries the risk of more severe memory and cognitive deficits.[2] Conversely, less aggressive resection reduces the risk of cognitive deficits but also reduces the likelihood of complete seizure freedom.[2] In addition to the procedures listed above, intraoperative electrocorticography (ECoG) is sometimes used to perform a more tailored resection of the hippocampus, however the prognostic value of this method remains controversial.[2]

The purpose of this study was to apply 7T tractography in epilepsy patients in a subfield-specific manner to measure subtle hippocampal connectomic changes that may occur as part of their disease profiles. Although the hippocampus is primarily composed of gray matter it also contains white matter neurocircuitry that project to limbic and cortical regions, and *ex vivo* rodent studies have suggested that different regions of the hippocampus exhibit distinct diffusion profiles.[14] In this study, we investigate hippocampal subfield connectivity related to the suspected seizure foci. Subfield-specific connectivity findings have not yet been reported in epilepsy patients *in vivo*, but may provide insight into the anatomy of the seizure network, as well as provide valuable clinical information that could be used to help guide surgical intervention and predict outcomes. In particular, using markers of connectivity that can be quantified with dMRI may present a novel method of profiling abnormalities within certain hippocampal subregions, and help guide placement sites of both intracranial electrodes and tissue resection in epilepsy patients considered MRI-negative by conventional imaging techniques.

2. Methods

2.1. Participants

Twenty-five focal epilepsy patients [16 females with mean age of 31.2 years, standard deviation (SD) 8.7 years; 9 males, mean 33.9 years, SD 14.4 years] were recruited through their neurologist at the Epilepsy Center at Mount Sinai Medical Center. All patients were MRI-negative, without abnormality on preceding clinical scans (1.5 or 3 T) and were drug resistant. Suspected seizure focus, EEG data, and postsurgical Engel score[24] for patients who have undergone surgery are provided in Table 1. Patients were age- and gender-matched with neurologically and psychiatrically healthy control participants [16 females: mean 31.7 years, SD 8.1 years; 9 males; mean 34.7 years, SD 12.5 years]. All participants provided written informed consent at the beginning of the study.

2.2. Imaging protocol

All participants were scanned under an Institutional Review Board-approved protocol using a 7T whole body scanner (Magnetom, Siemens Healthcare, Erlangen, Germany). A SC72CD gradient coil was used (G_{max} = 70 mT/m, max slew rate = 200T/m/s), with a single channel transmit and 32-channel receive head coil (Nova Medical, Wilmington, MA, USA). The MRI scan included a T_1-weighted MP2RAGE sequence: TR = 6000 ms, TE = 3.62 ms, flip angle = 5°, field of view = 240 × 320 mm^2, slices = 240, 0.7 mm^3 isotropic resolution, scan time = 7:26 min. A coronal-oblique T_2-weighted turbo spin echo (T_2TSE) sequence was included: TR = 6900 ms, TE = 69 ms, flip angle = 150°, field of view = 202 × 202 mm^2, in-plane resolution 0.4 × 0.4 mm^2, slice thickness = 2 mm, slices = 40, time = 6:14 min. A high-angular-resolved diffusion-weighted imaging (HARDI) dMRI sequence was also performed with whole-brain coverage: b = 1200 s/mm^2, TR = 7200 ms, TE = 67.6 ms, 1.05 mm isotropic resolution, in-plane acceleration R = 3 (GRAPPA), reversed phase encoding in the AP and PA direction for paired acquisition in 68 directions, with a total acquisition time of 20 minutes.

2.3. Hippocampal subfield segmentation

Automated cortical reconstruction was performed on the T_1-weighted images using the ‘recon-all’ function in the Freesurfer (http://surfer.nmr.mgh.harvard.edu) image analysis suite version 6.0. After completing the cortical reconstruction, a multispectral segmentation of the hippocampal subfields[18] was performed using both the T_1-weighted and the T_2weighted images (Figure 1). The following subfields were segmented: subiculum, presubiculum, parasubiculum; CA1, CA3, CA4; hippocampal tail, hippocampal fissure; molecular layer, granule cell layer of dentate gyrus (GC-ML-DG), fimbria, hippocampal-amygdala transition area (HATA); and the whole hippocampus. Hippocampal subfield volumes were co-registered using nearest neighbor interpolation to dMRI images using Statistical Parametric Mapping 12 (SPM) in MATLAB (r2017a, The MathWorks, Natick, MA). Qualitative manual inspection of the subfield volumes was performed to ensure proper segmentation and co-registration was achieved.

2.4. dMRI processing

The dMRI pre-processing was done using the human connectome project (HCP) pipelines, adjusted to account for significant eddy currents. The pre-processing pipeline included skull-stripping, eddy current correction using FMRIB Software Library (FSL) (www.fmrib.ox.ac.uk/fsl)[25], correction of gradient non-linearities using the HCP, and coregistration to the structural images from the Freesurfer pipeline. A 5-tissue segmentation of the T1-weighted image into gray matter, white matter, ventricles, non-ventricular cerebrospinal fluid and lesion(s) was performed using Freesurfer. This segmentation was used to create a grey-white matter mask, which was used to seed the anatomically constrained tractography. Constrained spherical deconvolution was used to calculate the fiber orientation distributions, and tensor metrics were obtained throughout the whole brain using MRtrix3 (Brain Research Institute, Melbourne, VIC, Australia). Whole-brain probabilistic tractography was performed using the iFOD2[26] algorithm and SIFT in MRtrix3 to select 10 million streamlines. Whole-brain structural connectivity matrices were then generated. The default '3dcalc' function in AFNI[27] was then used to modify the standard Freesurfer parcellation image (Desikan-Killiany atlas) to substitute the constitutive hippocampal subfields for the whole hippocampus. The modified parcellation image was used to construct connectivity matrices that contained the number of streamlines between each hippocampal subfield and the rest of the brain. The workflow of the diffusion processing is shown in Figure 2. The degree of each subfield was determined by calculating the total number of streamlines connecting a particular subfield with every other region of the brain. The fiber densities of the subfields were then calculated by dividing the degree of the subfield by the subfield volume.

2.5. Statistical analysis

Statistical analyses were performed using SAS v9.4 (SAS Institute Inc, Cary, NC). The degrees of connectivity and the fiber densities of i) the total epilepsy group, ii) the temporal onset subgroup, iii) the *left* temporal onset subgroup, and iv) *right* temporal onset subgroup were all compared against healthy controls. Epilepsy subjects were individually matched with healthy control subjects with respect to age and gender. The within-pair difference was calculated for each subfield variable and then tested for whether the location of the median was zero using the two-tailed sign-rank test. The false discovery rate (FDR) correction for multiple comparisons was performed post-hoc. A p-value ≤ 0.05 after the FDR correction was considered significant.

3. Results

3.1. Degree analyses of hippocampal subfields

A 3-dimensional rendering of the tractography is shown in Figure 3. Table 2 contains the hippocampal subfield degrees of connectivity. For the entire epilepsy group, the whole right hippocampus was significantly reduced in degree of connectivity ($p = 0.03$). The temporal onset group also showed reduced degree of connectivity in the whole right hippocampus ($p = 0.05$). Lastly, the left temporal onset group showed increased degree of connectivity in the left parasubiculum ($p = 0.04$) and presubiculum ($p = 0.04$) as well as reduced degree of

connectivity in the right subiculum (p = 0.04), CA1 (p = 0.03), and whole right hippocampus (p = 0.03). No significant effects were observed in the right temporal onset group (n = 5).

3.2. Fiber density analyses of hippocampal subfields

Table 3 presents the fiber densities of each hippocampal subfield. The entire epilepsy group showed increased fiber density in the left presubiculum (p = 0.02). The left temporal onset group showed increased fiber density in the left subiculum (p = 0.05), presubiculum (p = 0.03), parasubiculum (p = 0.03), CA3 (p = 0.04), and CA4 (p = 0.04) as well as reduced fiber density in the right subiculum (p = 0.02), CA1 (p = 0.05) and whole hippocampus (p = 0.05). The temporal and right temporal onset groups showed no significant effects.

Discussion

We present a novel method of hippocampal subfield-specific tractography that we used to quantify structural connectivity of the hippocampal subfields in epilepsy patients who were MRI-negative at clinical field strengths. We leveraged the high isotropic dMRI enabled by 7T MRI to probe the connectivity of the individual subfields with the hypothesis that their distinct cellular compositions may render some subfields more affected than others in epilepsy patients. Our results contribute to growing evidence that the subregions of the hippocampus are differentially affected in epilepsy.[19,20,28] While high-resolution dMRI has been used to perform tractography if the hippocampal subfields in rodent studies[14], this is the first attempt to quantify subfield connectivity in epilepsy patients. The use of ultra-high field MRI to facilitate accurate segmentation of the hippocampus and to enable high-resolution dMRI could be valuable in research and clinical settings, not only with improving our understanding of the seizure anatomy of MRI-negative epilepsy, but also in providing novel information that could influence seizure focus hypothesis and inform neurosurgical intervention.

In the present study, we observed an increase in both degree of connectivity and fiber density of some left subfields in the patients with suspected foci in the left temporal lobe. While the entire epilepsy group also showed increased fiber density in the left presubiculum, the finding of increased connectivity in left subfields was most apparent in the left temporal patients. These patients exhibited increased degree of connectivity in the left presubiculum and parasubiculum, and increased fiber density in the left presubiculum, parasubiculum, and subiculum. The mechanisms behind epileptogenic activity are not fully understood, although there is evidence suggesting that DRE patients experience synaptic reorganization within certain cortical structures, such as the hippocampus. This restructuring of hippocampal circuitry is believed to contribute to synchronization of electrical activity between subfields, as well as hyperexcitability of the hippocampus. While mossy fiber sprouting within the dentate gyrus has been well documented, there is evidence that other hippocampal regions exhibit comparable reorganization in response to excitotoxic seizures.[29] Since the subicular complex is the main output of the hippocampal formation, its reorganization could contribute to seizure propagation and affect the switch between interictal and ictal activity.[29] Increased lamellar interconnectivity of the subicular complex with other subfields is believed to play an important role in synchronization of the hippocampal subfields.[29] Restructuring of

the subicular regions consequent to repeated electrical insult could explain our finding of increased connectivity of the presubiculum, parasubiculum, and subiculum on the side of suspected seizure onset, and this report of increased connectivity among these regions *in vivo* is the first we are aware of. Further analysis with a larger sample size will be needed to corroborate this finding. Similar validation will be needed to confirm our findings of increased fiber density within the left CA3 and CA4 of left temporal onset patients, although these findings may instead reflect volume reduction in these two subfields, as they were not increased in degree of connectivity.

Conversely, left temporal patients showed reduced degree of connectivity and fiber density in the right subiculum, CA1, and the whole right hippocampus. Both the temporal onset group and entire epilepsy cohort also displayed reduced connectivity in the whole right hippocampus. Vulnerability of particular cell types to seizure-induced damage has been reported in certain hippocampal subfields.[30] Two subclasses of GABAergic interneurons, the somatostatin- and parvalbumin-expressing neurons, responsible for dendritic and perisomatic inhibition respectively, are susceptible to excitotoxic damage in temporal lobe epilepsy.[31] These neurons are mainly located in the hilus of the dentate gyrus and the stratum oriens of CA1, which could explain our finding of reduced degree of connectivity and fiber density of CA1.[32] Other studies have shown that CA1 is particularly vulnerable to seizure-induced damage[33]. Interestingly, reduced CA1 connectivity was only observed contralateral to the suspected seizure focus in left temporal patients. Scanning more patients with temporal epilepsy will help to establish the mechanisms behind our overall finding of reduced connectivity of certain subfields contralateral to the suspected seizure focus, namely the subiculum and CA1, and increased connectivity of some subfields ipsilateral to the suspected seizure focus, especially as the subiculum, presubiculum, and parasubiculum.

The findings presented in this study may have important applications in neurosurgical planning. The extent of temporal lobe resection in epilepsy surgery varies between surgeons, and it is difficult to achieve the optimal balance of seizure freedom and preservation of cognitive function.[2] The present study offers hippocampal subfield-specific tractography as a novel imaging-based method that may provide advanced information about the connectivity and microstructure of the hippocampal subfields, potentially sparing non-implicated regions of the hippocampus or temporal lobe from resection. The results presented in this study may also benefit the planning of placement sites for intracranial electrode surgeries, since intracranial monitoring procedures employ minimally invasive techniques, and each additional electrode increases the risk of complications by only 0.18%.[34] Information about the structural connectivity of the hippocampal subfields provided by dMRI could help inform placement sites for SEEG electrodes by implicating regions of the hippocampus that otherwise appeared normal on presurgical imaging. Future investigation of this topic would benefit from precise placement of SEEG electrodes into hippocampal subfields shown to have significantly increased or decreased connectivity. Additionally, determining whether the extent of subfield connectivity alteration correlates with severity and/or duration of disease would be valuable, and is an area of future investigation.

The logistical challenge of scanning non-lesional patients at 7T resulted in a relatively low number of participants, especially considering the heterogeneity of epilepsy types

investigated, which was the primary limitation of this study. Future investigations will include larger sample sizes in all seizure onset groups to ensure greater statistical power. We are also unable to discern whether the findings observed in this study were an effect of epilepsy or whether they were underlying causes that made the participants susceptible to seizure activity. One of the major findings in this study was increased connectivity of the major output gate of the hippocampus, the subicular complex, on the side of suspected seizure onset in left temporal epilepsy patients. Whether this is the main mechanism behind seizure activity in these patients, or merely a result of repeated electrical insult, is unknown and is an area of active investigation. Lastly, although dMRI-based tractography is progressively being incorporated into surgical planning, the technique has its own limitations, such as false positives partial volume effects. While these drawbacks are inherent to investigations of small structures such as the hippocampal subfields, we believe that the high spatial dMRI resolution minimized partial volume effects and allowed for an accurate first assessment of subfield connectivity in epilepsy patients. However, comparison with electrophysiology is still necessary to validate dMRI-based tractography findings and establish adequate reliability of this method to guide seizure hypothesis and neurosurgery.[35]

Conclusions

The predictive association between an identifiable hippocampal lesion, such as hippocampal sclerosis, and postsurgical seizure freedom in epilepsy patients has generated interest in developing novel methods of identifying ‘abnormality’ beyond traditional imaging protocols. A growing body of research suggests that despite normal appearing clinical scans, abnormalities may be detected in MRI-negative patients using advanced imaging techniques.[19,20,36] Indeed, there is much interest among seizure imaging researchers regarding the applications of ultra-high field MRI and advanced imaging modalities such as dMRI, functional MRI and magnetic resonance spectroscopy imaging to detect potential seizure foci in MRI-negative patients.[20,36,37] MRI-negative patients with poorly understood epileptogenic foci could benefit from novel markers of abnormality that provide more accurate information than traditional imaging methods. In this study we aimed to measure the degree and fiber density of individual hippocampal subfields to quantify the overall connectivity of each. Despite being MRI-negative, the patients in this study revealed strong effects within certain hippocampal subfields. For seizure patients with non-diagnostic clinical imaging, ultra-high field MRI might generate sufficiently high-resolution structural images that permit delineation of hippocampal subfield boundaries to i) guide high-resolution dMRI, and ii) measure the connectivity of the hippocampal subfields. Novel imaging modalities such as dMRI hold the potential to reveal subtle abnormalities not detectable with current clinical methods, which could aid in seizure focus hypothesis and influence neurosurgical intervention.

Acknowledgments

Funding

NIH R00 NS070821

NIH R01 CA202911

NIH R01 MH109544

NARSAD Young Investigator Grant

Icahn School of Medicine Capital Campaign, Translational and Molecular Imaging Institute and Department of Radiology, Icahn School of Medicine at Mount Sinai, Siemens Healthcare

Dr. Balchandani has received support from NIH R01 MH109544, NIH-NINDS R00 NS070821; Icahn School of Medicine Capital Campaign, Translational and Molecular Imaging Institute and Department of Radiology, Icahn School of Medicine at Mount Sinai, Siemens Healthcare

References

1. Epilepsy in Adults and Access to Care — United States. Center for Disease Control and Prevention 2010.
2. Jobst BC, Cascino GD. Resective Epilepsy Surgery for Drug-Resistant Focal Epilepsy A Review. JAMA 2015; 313:285–93. [PubMed: 25602999]
3. Duncan JS, Sander JW, Sisodiya SM, et al. Adult epilepsy. Lancet 2006; 367:1087–1100. [PubMed: 16581409]
4. Kwan P, Brodie MJ. Early identification of refractory epilepsy. N Engl J Med 2000; 342:314–319. [PubMed: 10660394]
5. Tellez-Zenteno JF, Dhar R, Hernandez-Ronquillo L, et al. Long-term outcomes in epilepsy surgery: antiepileptic drugs, mortality, cognitive and psychosocial aspects. Brain 2007; 130:334–345. [PubMed: 17124190]
6. Nowell M, Miserocchi A, McEvoy AW, et al. Advances in epilepsy surgery. J Neurol Neurosurg Psychiatry 2014; 85:1273–1279. [PubMed: 24719180]
7. McGonigal A, Bartolomei F, Régis J, Guye M, Gavaret M, Trébuchon-Da Fonseca A, Dufour H, Figarella-Branger D, Girard N, Péragut JC, Chauvel P. Stereoelectroencephalography in presurgical assessment of MRI-negative epilepsy. Brain 2007; 130:12, 3169–3183. [PubMed: 17855377]
8. Duncan JS, Sander JW, Sisodiya SM, et al. Adult epilepsy. Lancet 2006; 367:1087–1100. [PubMed: 16581409]
9. Nguyen DK, Mbacfou MT, Nguyen DB, et al. Prevalence of nonlesional focal epilepsy in an adult epilepsy clinic. Can J Neurol Sci 2013; 40:198–202. [PubMed: 23419568]
10. Winston GP, Micallef C, Kendell BE, et al. The value of repeat neuroimaging forepilepsy at a tertiary referral centre: 16 years of experience. Epilepsy Res 2013; 105:349355.
11. Téllez-Zenteno JF, Dhar R, Wiebe S. Long-term seizure outcomes following epilepsy surgery: a systematic review and meta-analysis. Brain 2005; 128: 5, 1188–1198. [PubMed: 15758038]
12. Téllez-Zenteno JF, Dhar R, Wiebe S. Long-term seizure outcomes following epilepsy surgery: a systematic review and meta-analysis. Brain 2005; 128:1188–98. [PubMed: 15758038]
13. Nair D, Burgess R, McIntyre C, Lüders H. Chronic subdural electrodes in the management of epilepsy. Clinical Neurophysiology 2008; 119:1, 11–28. [PubMed: 18035590]
14. Shepherd TM, Ozarslan E, King MA, Mareci TH, Blackband SJ. Structural insightsfrom high-resolution diffusion tensor imaging and tractography of the isolated rat hippocampus. NeuroImage 2006 32: 1499–1509. [PubMed: 16806988]
15. James GA, Tripathi SP, Ojemann JG, Gross RE, Drane DL. Diminished default mode network recruitment of the hippocampus and parahippocampus in temporal lobe epilepsy. Journal of Neurosurgery 2013; 119:288–300. [PubMed: 23706058]
16. Voets NL, Beckmann CF, Cole DM, Hong S, Bernasconi A, Bernasconi N. Structural substrates for resting network disruption in temporal lobe epilepsy. Brain 2012; 135:2350–7. [PubMed: 22669081]
17. Schoene-Bake JC, Keller SS, Niehusmann P, Volmering E, Elger C, Deppe M, Weber B. In vivo mapping of hippocampal subfields in mesial temporal lobe epilepsy: Relation to histopathology. Human Brain Mapping 2014; 35:9, 4718–4728.

18. Iglesias JE, Augustinack JC, Nguyen K, Player CM, Player Wright M, Roy N, Frosch MP, McKee AC, Wald LL, Fisch B, Van Leemput KA. Computational atlas of the hippocampal formation using ex vivo, ultra-high resolution MRI: Application to adaptive segmentation of in vivo MRI. Neuroimage 2015; 115, 117–137. [PubMed: 25936807]
19. Sone D, Sato N, Maikusa N, Ota M, Sumida K, Yokoyama K, Kimura Y, Imabayashi E, Watanabe Y, Watanabe M, Okazaki M, Onuma T, Matsuda H. Automated subfield volumetric analysis of hippocampus in temporal lobe epilepsy using high-resolution T2weighed MR imaging. Neuroimage Clinical 2016; 12: 57–64. [PubMed: 27489767]
20. Voets NL, Hodgetts CJ, Sen A, Adcock JE, Emir U. Hippocampal MRS and subfield volumetry at 7T detects dysfunction not specific to seizure focus. Scientific Reports 2017; 7:16138. [PubMed: 29170537]
21. Fock NK, Yogara M, Bonelli SB, Bartlett PA, Symms MR, Duncan JS. Voxel-based diffusion tensor imaging in patients with mesial temporal lobe epilepsy and hippocampal sclerosis. Neuroimage 2008; 1;40:728–737.
22. Le Bihan D, Mangin JF, Poupon C, Clark CA, Pappata S, Molko N, Chabriat H. Diffusion tensor imaging: Concepts and applications. J Magn Reson Imaging 2001; 13:534–46. [PubMed: 11276097]
23. Polders DL. Signal to noise ratio and uncertainty in diffusion tensor imaging at 1.5, 3.0,and 7.0 Tesla. J Magn Reson Imaging 2011; 33:1456–63. [PubMed: 21591016]
24. Engel J,, Jr. Update on surgical treatment of the epilepsies. Summary of the Second International Palm Desert Conference on the Surgical Treatment of the Epilepsies. Neurology 1993; 43: 1612–1617. [PubMed: 8102482]
25. Woolrich MW, Jbabdi S, Patenaude B, Chappell M, Makni S, Behrens T, Beckmann C, Jenkinson M, Smith SM. Bayesian analysis of neuroimaging data in FSL. NeuroImage 2009; 45:S173–86. [PubMed: 19059349]
26. Tournier J, Calamante F, Connelly A. Improved probabilistic streamlines tractography by 2nd order integration over fibre orientation distributions. In: Proc. 18th Annual Meeting of the Intl. Soc. Mag. Reson. Med ISMRM 2010, 1670 Abstract.
27. Cox RW. AFNI: software for analysis and visualization of functional magnetic resonance neuroimages. Comput Biomed Res 1996; 29: 162–173. [PubMed: 8812068]
28. Lemkaddem A, Daducci A, Kunz N, Lazeyras F, Seeck M, Thiran JP, Vulliemoz S. Connectivity and tissue microstructural alterations in right and left temporal lobe epilepsy revealed by diffusion spectrum imaging. NeuroImage Clinical 2014; 5:349–358. [PubMed: 26236626]
29. Cavazos JE, Cross DJ. The role of synaptic reorganization in mesial temporal lobe. Epilepsy Behavior 2006; 8:483–493. [PubMed: 16500154]
30. Gorter JA, van Vliet EA, Aronica E, Lopes da Silva FH. Progression of spontaneous seizures after status epilepticus is associated with mossy fibre sprouting and extensive bilateral loss of hilar parvalbumin and somatostatin-immunoreactive neurons. Eur J Neurosci 2001; 13: 657–669. [PubMed: 11207801]
31. Dinocourt C,
Petanjek Z,
Freund TF,
Ben-Ari Y,
Esclapez M. Loss of interneurons innervating pyramidal cell dendrites and axon initial segments in the CA1 region of the hippocampus following pilocarpine-induced seizures. Journal of Comparative Neurology 2003; 459:407–25.
32. Andre V, Marescaux C, Nehlig A, Fritschy JM. Alterations of hippocampal GABAergic system contribute to development of spontaneous recurrent seizures in the rat lithium-pilocarpine model of temporal lobe epilepsy. Hippocampus 2001; 11: 452–468. [PubMed: 11530850]
33. Wasterlain CG, Treiman DM. Status Epilepticus: Mechanisms and Management. MIT Press; 2006.
34. Gonzalez-Martin J, Mullin J, Vadera S, Bulacio J, Hughes G, Jones S, Enatsu R,Najam I. Stereotactic placement of depth electrodes in medically intractable epilepsy. Journal of Neurosurgery 2014; 120:639–644. [PubMed: 24405074]

35. Gomes J, Gorgulho A, de Oliveira Lopez A, Saraiva C, Damiani L, Passaro A, Salvajoli J, de Oliveira Siqueira L, Salvajoli B, De Salles A. The role of diffusion tensor imaging tractography for Gamma Knife thalamotomy planning. Journal of Neurosurgery 2016; 125:129–138. [PubMed: 27903188]

36. Veersema TJ, Ferrier CH, van Eijsden P, Gosselaar PH, Aronica E, Visser F, Zwanenburg JM, de Kort G, Hendrikse J, Luijten PR, Braun K. Seven tesla MRI improves detection of focal cortical dysplasia in patients with refractory focal epilepsy. Epilepsia Open 2017; 2: 162–171 [PubMed: 29588945]

37. Maccotta L, Moseley ED, Benzinger TL, Hogan RE. Beyond the CA1 subfield: Local hippocampal shape changes in MRI-negative temporal lobe epilepsy. Epilepsia 2015; 56: 780–788. [PubMed: 25809286]

Highlights

- High-resolution dMRI enables subfield-specific tractography in the hippocampus.
- Subfield tractography may detect subtle connectivity changes in MRI-negative patients
- Left temporal lobe epilepsy patients show increased ipsilateral connectivity
- Hippocampal subfield-specific tractography may be a useful technique to predict seizure focus

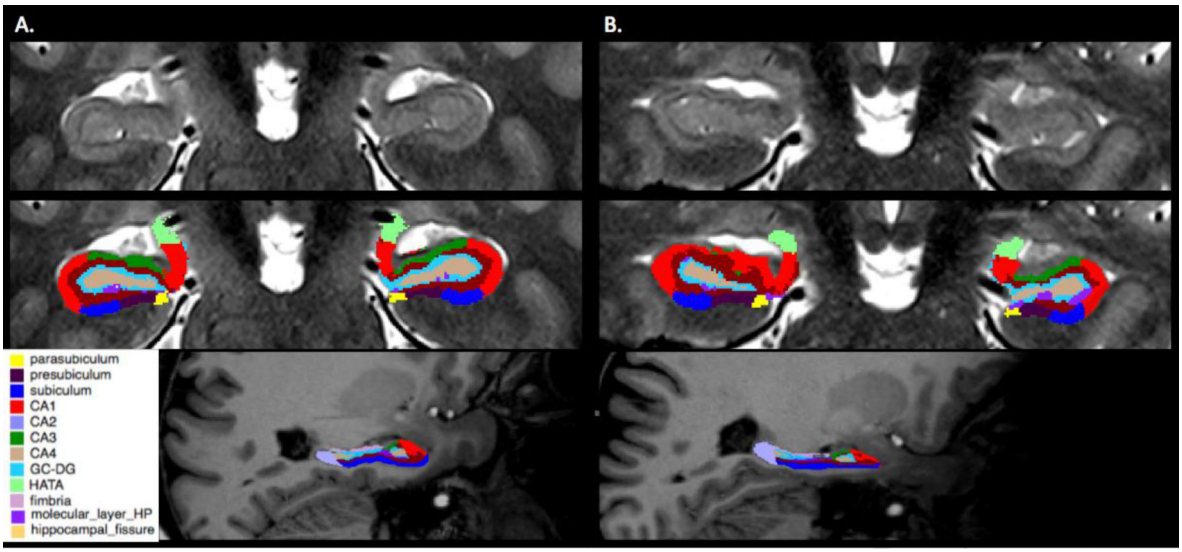

Figure 1.

Examples of automated hippocampal subfield segmentation derived from Freesurfer version 6.0 in a healthy control (column A) and an epilepsy patient (column B). Row 1 contains unlabeled coronal mid- hippocampal sections on a T2-weighted image. Row 2 shows the same sections with colored subfield overlays. Row 3 exhibits sagittal color overlay representations on a T1-weighted image with anterior to the reader's right. CA4 corresponds to the hilar portion of the CA3 field.

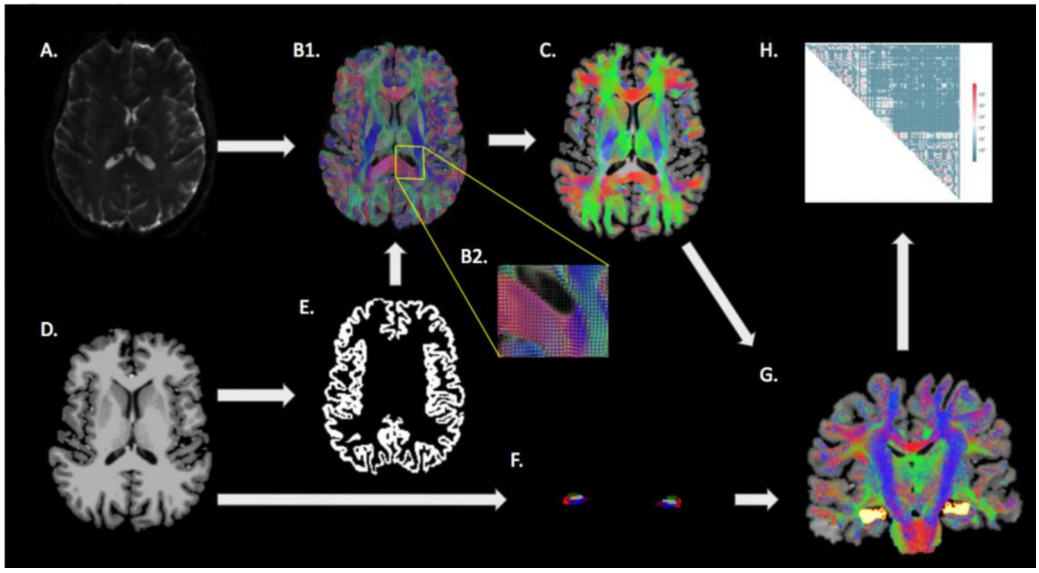

Figure 2.

A schematic of the semi-automated tractography and hippocampal subfield fiber density calculation workflow. The dMRI image (A) was used to derive the fiber orientation distribution image (B1, with magnification inset B2), which was then used to perform whole-brain probabilistic tractography (C). The T1- weighted anatomical image (D) was used to determine the gray matter-white matter boundary (E) and to segment the hippocampal subfields (F). The hippocampal subfields were defined as seed points for tractography of the individual subfields (G) from which connectomes were defined (H).

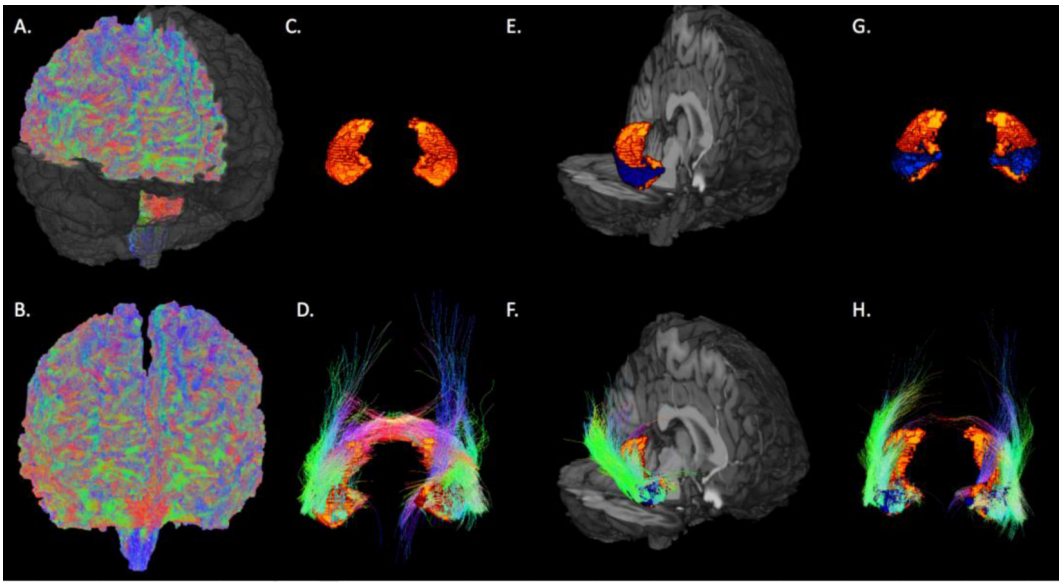

Figure 3.

Healthy control. Examples of whole-brain probabilistic tractography (quadratic surface erosion in A, global surface erosion in B), bilateral hippocampi volumes (C.), fibers from both hippocampi (D.), CA1 (blue) within the right hippocampus (E.), fibers from right CA1 (F.), bilateral CA1 (G.), and fibers from bilateral CA1 (H).

Table 1.

Patient EEG data and suspected seizure foci. L: Left, R: Right, B/L: Bilateral, GTCC: generalized tonic clonic convulsions, GRDA: generalized rhythmic delta activity, BIRD: brief potentially ictal rhythmic discharges

Subject	Gender	Age at scan (years)	Suspected seizure focus	EEG Results	Engel Score
1	M	64	L_Frontal	Diffuse rhythmic theta Multiple seizures with decreased responsiveness with diffuse theta 1 GTCC not lateralizable electrographically	N/A
2	M	23	R_Temporal	Rare R anterior temporal spikes	1
3	F	33	L_Temporal	Abundant b/l central spikes more prominent on the L Intracranial EEG: B/l spiking 12 seizures of onset within left parietal lesion Rapid spread	1
4	F	32	L_Temporal	L posterior quadrant	N/A
5	F	28	Unknown	Background normal Seizure onset diffusion Better development on L	N/A
6	F	27	R_Temporal/Frontal	Occasional R temporal slowing Frequent R temporal sharp waves Multiple seizure R -sided onset some temporal, some central	N/A
7	F	27	L_Temporal	L FT slowing L temporal quasi-periodic sharp waves L anterior temporal LRDA 3 seizures of L temporal origin	N/A
8	F	22	L_Temporal/Frontal	Rare L temporal sharp waves 5 seizures: 4 with L FT onset; 1 unlateralized	N/A
9	F	21	R_Temporal	R anterior slowing GRDA 2 seizures of R temporal onset	N/A
10	F	47	B/L_Temporal	B/l FT slowing B/l temporal sharp waves Unclear electrographic onset (one R and one L)	N/A
11	F	34	B/L_Temporal	B/l slowing B/l temporal sharp waves Multiple seizure captured, non-lateralizable Intracranial EEG: b/l independent mesial temporal onset	2
12	M	23	Unknown	Recent -> normal Past -> multi-focal discharges	N/A
13	M	29	Unknown	Normal	N/A
14	F	46	L_Temporal	L anterior temporal sharp waves Intermittent bi-temporal slowing L temporal seizures	N/A
15	F	28	L_Frontal	Frequent L central spikes Seizures are EEG negative	N/A
16	M	30	L_Temporal/Parieta l	Occasional L parietal BIRD Rare L parietal spikes Seizure not captured	N/A
17	M	29	L_Temporal/Frontal	Frequent L FT slowing Occasional L FT spikes	N/A
18	F	47	L_Temporal	No slowing, L temporal spikes L temporal seizure	N/A
19	F	24	B/L _Temporal	Focal to bilateral tonic clonic Mild generalized slowing R temporal slowing	N/A
20	F	32	R_Temporal	anterior temporal spikes R temporal seizures captured	N/A
21	M	51	B/L_Temporal	L anterior quadrant seizure	2
22	M	21	R_Temporal/Frontal	R fronto-temporal slowing R fronto-temporal sharp waves R fronto-temporal spikes	N/A
23	M	35	Unknown	Normal	N/A
24	F	30	B/L_Temporal	L temporal slowing L anterior temporal spikes R posterior temporal spikes	N/A
25	F	21	L_Temporal	L hemisphere slowing L centrotemporal spikes Seizures of left side origin	N/A

Table 2.

Mean (standard deviation) degrees of connectivity among hippocampal subfields

	All patients (n=25)	Temporal Onset (n=19)	Left Temporal Onset (n=9)	Right Temporal Onset (n=5)	Control (n=25)
Left Hemisphere					
Tail	4238.2 (2007.3)	1378 (1943.1)	4792.1 (1730.9)	3677.4 (1871.4)	3863.87 (2026.73)
Subiculum	4795.0 (1877.3)	4614.5 (1892)	4821.7 (2533.6)	4585.2 (1068.5)	4590.93 (2119.36)
CA1	1413.4 (463.1)	1377 (473.7)	1416.8 (443.8)	1252.6 (505.6)	1429.92 (578.12)
Fissure	50 (118.4)	58.6 (135.1)	22.1 (29.2)	141.6 (244.7)	55.54 (132.93)
Presubiculum	537.0 (449.3)	500.9 (451)	*__801.6__ (487.7)	301.3 (172.4)	281.46 (151.17)
Parasubiculum	2034.2 (1036.8)	1963.3 (1038.6)	*__2429.8__ (1072)	1527.4 (931.6)	1697.25 (1102.26)
Molecular layer	776.1 (338.7)	740.5 (309.3)	812 (360.5)	707.4 (288.4)	821.10 (294.88)
GC-ML-DG	97.1 (130.3)	79.1 (106.9)	55.2 (47.8)	139.9 (195.2)	117.45 (121.48)
CA3	1948.1 (1106.4)	1926.6 (1158.6)	2402.4 (1131.8)	1439.4 (1202.5)	1829.60 (866.85)
CA4	2183.6 (884.1)	2227.3 (942.8)	2738.3 (957.5)	1532.6 (846.4)	2475.99 (805.23)
Fimbria	539 (328.2)	578 (306.4)	601.4 (301.8)	651.4 (426.1)	583.37 (516.12)
HATA	447.2 (368.1)	427 (359.8)	593.5 (454.5)	221.7 (68.2)	501.63 (221.96)
Whole Hippocampus	19058.8 (5991.3)	18869.3 (5787.5)	21486.8 (5724.9)	16177.7 (4196.2)	18248.10 (6231.95)
Right Hemisphere					
Tail	13205.4 (6836.1)	13666 (7012.7)	13986.3 (6321.8)	12507.2 (9830.4)	17956.79 (8015.10)
Subiculum	14771.2 (6438.7)	14381.2 (6740.4)	*__13757.4__ (6224)	12971.1 (8650)	18771.71 (6327.82)
CA1	8149.8 (3816.4)	7965.8 (3825.8)	*__7138.7__ (2073.7)	6593.4 (5260.9)	10985.91 (5234.06)
Fissure	291.6 (323.9)	307.8 (361.5)	222.7 (200.7)	195.3 (234.3)	211.50 (284.59)
Presubiculum	856 (528.3)	831.9 (527.7)	929.9 (465.9)	615.5 (264.6)	880.90 (1310.40)
Parasubiculum	3659.2 (4356.4)	2743.6 (1269.5)	3056.6 (1500.4)	2125.2 (1106.6)	3288.33 (2787.60)
Molecular layer	2072.12 (754.5)	2024 (755)	2246.7 (518.8)	2047.1 (1245.4)	1933.72 (1273.73)
GC-ML-DG	232 (198.8)	226.5 (171.9)	252 (176.4)	277 (226.4)	330.74 (394.45)
CA3	4013.5 (2431.4	3921.4 (2680.5)	3680.4 (1562.6)	4600.4 (5022.5)	3832.79 (2302.43)
CA4	9078 (3500.3)	9255.4 (3764.2)	9245.4 (1581.2)	7258.5 (4079.6)	10565.31 (5115.32)
Fimbria	1184 (619.4)	1123.3 (557.5)	1033.8 (366.7)	1204.4 (890.3)	1235.38 (706.49)
HATA	487.3 (262.5)	524.6 (286.53)	539.7 (283.8)	441.5 (98.2)	631.80 (442.95)
Whole Hippocampus	*__58000.2__ (19307)	*__56971.3__ (21043.2)	*__56089.5__ (14507.5)	50836.4 (34566.7)	72332.09 (19717.45)

*significant after FDR correction, CA: Cornu Ammonis, GC-ML-DG: granule cell layer of dentate gyrus, HATA: hippocampal-amygdala transition area

Table 3.

Mean (standard deviation) fiber densities of hippocampal subfields

	All patients (n=25)	Temporal Onset (n=19)	Left Temporal Onset (n=9)	Right Temporal Onset (n=5)	Control (n=25)
Left Hemisphere					
Tail	9.99 (4.48)	10.14 (4.67)	11.57 (4.84)	8.65 (4.27)	9.06 (4.51)
Subiculum	14.35 (5.20)	13.39 (5.44)	*__14.28__ (7.01)	14.12 (4.01)	11.61 (5.22)
CA1	2.72 (0.86)	2.61 (0.74)	2.81 (0.67)	2.46 (0.90)	2.44 (1.12)
Fissure	0.44 (1.06)	0.53 (1.21)	0.20 (0.31)	1.30 (2.19)	0.52 (1.28)
Presubiculum	*__2.23__ (1.82)	2.09 (1.77)	*__3.35__ (1.76)	1.32 (0.75)	1.03 (0.57)
Parasubiculum	39.23 (21.42)	36.48 (20.05)	*__46.48__ (21.10)	29.27 (16.60)	27.12 (16.88)
Molecular layer	1.57 (0.73)	1.47 (0.66)	1.63 (0.73)	1.45 (0.67)	1.46 (0.44)
GC-ML-DG	0.42 (0.57)	0.35 (0.51)	0.20 (0.31)	0.66 (0.94)	0.46 (0.49)
CA3	11.61 (6.43)	11.22 (7.15)	*__14.48__ (6.60)	0.90 (8.06)	9.44 (4.53)
CA4	11.51 (4.18)	11.38 (4.55)	*__14.51__ (4.08)	7.88 (3.40)	11.65 (3.94)
Fimbria	7.94 (4.44)	8.29 (4.54)	9.14 (5.20)	9.65 (4.37)	6.46 (4.04)
HATA	8.62 (6.81)	8.05 (6.43)	11.39 (7.99)	4.68 (1.52)	9.38 (4.32)
Whole Hippocampus	6.70 (2.12)	6.68 (2.06)	7.83 (1.91)	5.93 (1.61)	5.79 (1.86)
Right Hemisphere					
Tail	34.98 (16.25)	34.82 (17.09)	34.77 (12.67)	33.89 (28.87)	40.03 (15.25)
Subiculum	42.15 (18.43)	41.96 (20.00)	*__39.18__ (15.62)	43.90 (32.31)	50.34 (18.28)
CA1	14.42 (7.39)	14.55 (7.84)	*__12.85__ (3.73)	14.60 (12.77)	18.87 (9.15)
Fissure	2.48 (2.70)	2.58 (2.90)	1.82 (1.81)	1.73 (2.00)	1.81 (2.70)
Presubiculum	3.62 (2.14)	3.60 (2.12)	4.01 (2.01)	3.23 (1.47)	3.41 (4.93)
Parasubiculum	66.70 (67.64)	53.90 (25.63)	61.84 (31.83)	45.39 (18.80)	59.33 (53.78)
Molecular layer	4.02 (1.74)	3.93 (1.80)	4.24 (0.96)	4.49 (3.18)	3.40 (2.31)
GC-ML-DG	1.03 (0.90)	1.06 (0.88)	1.15 (0.83)	1.46 (1.23)	1.37 (1.75)
CA3	22.18 (15.81)	22.07 (17.35)	19.56 (7.54)	29.06 (33.07)	20.32 (11.06)
CA4	46.65 (17.65)	48.55 (18.54)	48.47 (7.31)	43.80 (26.55)	52.59 (27.68)
Fimbria	18.92 (12.68)	19.19 (13.28)	17.48 (7.06)	23.65 (24.94)	16.25 (9.11)
HATA	8.89 (4.84)	9.77 (5.22)	10.00 (5.39)	8.89 (1.39)	11.33 (7.52)
Whole Hippocampus	20.47 (7.72)	20.41 (8.55)	*__19.77__ (4.94)	20.93 (15.95)	23.48 (6.64)

*significant after FDR correction, CA: Cornu Ammonis, GC-ML-DG: granule cell layer of dentate gyrus, HATA: hippocampal-amygdala transition area